Australasian Physical & Engineering Sciences in Medicine (2019) 42:503–510
https://doi.org/10.1007/s13246-019-00747-4

SCIENTIFIC PAPER

Effective temporal resolution and image quality of volume scanning in 320-row detector CT

Atsushi Urikura[1] · Takanori Hara[2] · Tsukasa Yoshida[3] · Eiji Nishimaru[4] · Takashi Hoshino[5] · Katsuhiro Ichikawa[6] · Yoshihiro Nakaya[1] · Masahiro Endo[1]

Received: 23 October 2018 / Accepted: 1 March 2019 / Published online: 7 March 2019

Abstract

To measure the effective temporal resolution (eTR) and image quality for three reconstruction modes for non-helical volume scanning in area detector CT. Temporal sensitivity profiles (TSPs) were obtained and the full width of the TSP at half maximum was used as an index of the eTR. Image quality was assessed by image noise and the corrected artifact index. The half reconstruction mode had a higher eTR than the full and automatic patient motion collection (APMC) reconstructions. Compared to full reconstruction, the image noise with APMC and half reconstruction were increased by 16% and 35%. The corrected artifact index was lowest with APMC. The square root of full width at tenth maximum of the TSP showed a high coefficient of determination ($R^2 = 0.934$) for image noise. This study revealed the TSPs and eTRs for non-helical volume scanning in area detector CT. A high eTR resulted in higher image noise.

Keywords Temporal resolution · Non-helical volume scanning · Computed tomography · Temporalsensitivity profiles · Motion artifact

Introduction

The development of high-speed data acquisition technology for multidetector-row computed tomography (MDCT) has allowed scanning at a high temporal resolution, thereby reducing motion artifact and blur in the acquired images [1, 2]. Recent studies have reported that

Advances in knowledge To our knowledge, this is the first study to assess the effective temporal resolution and TSP of volume scanning in an area detector CT. To maintain the image quality while reducing motion artifacts, the CT operator should determine the optimal reconstruction mode.

✉ Atsushi Urikura
at.urikura@scchr.jp

Takanori Hara
hara_tnk2@ybb.ne.jp

Tsukasa Yoshida
ts.yoshida@scchr.jp

Eiji Nishimaru
eiji2403@tk9.so-net.ne.jp

Takashi Hoshino
hoshi0311@hera.eonet.ne.jp

Katsuhiro Ichikawa
ichikawa@mhs.mp.kanazawa-u.ac.jp

Yoshihiro Nakaya
y.nakaya@scchr.jp

Masahiro Endo
m.endo@scchr.jp

[1] Division of Diagnostic Radiology, Shizuoka Cancer Center, 1007 Shimonagakubo, Nagaizumi, Sunto, Shizuoka 411-8777, Japan

[2] Department of Medical Technology, Nakatsugawa Municipal General Hospital, 1522-1 Komanba, Nakatsugawa, Gifu 508-0011, Japan

[3] Division of Radiation and Proton Therapy Center, Shizuoka Cancer Center, 1007 Shimonagakubo, Nagaizumi, Sunto, Shizuoka 411-8777, Japan

[4] Department of Radiology, Hiroshima University Hospital, 1-2-3, Kasumi, Minami-ku, Hiroshima 734-8551, Japan

[5] Department of Radiological Technology, Osaka College of High Technology, 1-2-8 Miyahara, Yodogawa-ku, Osaka, Osaka 532-0003, Japan

[6] Division of Health Sciences, Kanazawa University Graduate of Medical Sciences, 5-11-80 Kodatsuno, Kanazawa, Ishikawa 920-0942, Japan

advanced CT scanners with high temporal resolution can reduce image quality degradation caused by motion artifacts [3–5]. Ohashi et al. [5] demonstrated the optimal temporal resolution for coronary CT-angiography (CCTA) in dual-source CT, showing that images with a high temporal resolution of 83 ms significantly reduced coronary artery motion artifacts. Hutt et al. [6] evaluated the effect of cardiogenic artifacts on depiction of the bronchial wall. Using dual-source CT, they acquired images at temporal resolutions of 75 ms and 140 ms and showed by visual assessment that these images depicted 78% and 30% of bronchi without motion, respectively. They concluded that a high temporal resolution reduced cardiac motion artifacts on bronchial walls.

Taguchi et al. [7] proposed a method to apply temporal resolution as a quantitative index by using the temporal sensitivity profile (TSP) that corresponds to the helical interpolation and/or gantry rotation time. Their results showed that the temporal resolution of the helical acquisition was improved by optimizing the interpolation algorithm. In a previous study, we proposed a method for obtaining the TSP and effective temporal resolution (eTR) in helical scanning by using a temporal impulse signal [8]. Subsequent measurements obtained by helical acquisition using 320-row area detector computed tomography (ADCT) and dual-source CT demonstrated that eTR was remarkably different between the two scanners [9]. The results for helical acquisition indicated that the temporal resolution was dependent not only on rotation time and pitch factor but also on the interpolation algorithm used for the image reconstructions.

Non-helical volume scanning (NVS) allows longitudinal data acquisition with a wide range of up to 160 mm using ADCT. It has been reported that NVS is effective for examinations that require high temporal resolution, such as CCTA or for thoracic aortic aneurysm. It has also been reported that NVS is a useful scanning method for chest CT as it helps to suppress blurring of the bronchi and pulmonary vessels due to the heartbeat [10, 11]. Furthermore, it has been shown that the NVS in 320-row ADCT without step artifact and motion artifact is useful for thoracic imaging in neonates and small children [12, 13].

The 320-row ADCT scanner has three types of reconstruction mode for NVS: full, half, and automatic patient motion correction (APMC). Although the APMC and half reconstruction modes are used to improve the temporal resolution in imaging such as CCTA, the eTR values for the images reconstructed with the three modes have not yet been fully established; to the best of our knowledge, no study has assessed eTRs for the three non-helical scanning reconstruction modes for 320-row ADCT. However, knowing the eTR and image quality for the NVS reconstruction modes is important for determining the scan parameters in clinical examinations, such as CCTA, chest, and pediatric CT.

The aims of this study were to measure the eTRs for NVS with a 320-row ADCT scanner and the three reconstruction modes, and to investigate the relationship between TSP and image quality.

Methods and materials

Data acquisition

The examinations were performed with volume scan mode installed in a second-generation ADCT scanner (Aquilion ONE ViSION Edition, Canon Medical Systems, Tokyo, Japan). The NVS acquisition parameters were as follows: 120 kVp, 200 mA, 0.5-mm thickness, detector configuration of 320×0.5 mm, and the FC01 reconstruction kernel. All images were reconstructed using the full, APMC, and half modes. The TSP and image qualities were measured with gantry rotation times of 275 and 400 ms. For the TSP measurement, the reconstruction time interval was set at 10 and 20 ms for the 275 and 400 ms gantry rotation times, respectively. The display field of view was adjusted 100 mm for TSP and 320 mm for the artifact index and image noise measurements.

Measurement of TSP and eTR using an impulse method

In a previous study, we showed that temporal resolution in helical acquisition could be measured by using a temporal impulse signal, firing a metal ball at high speed in a direction vertical to the slice plane and using the intensity of the streak artifacts generated by this to produce the TSP [8]. In helical scanning, images with short time intervals disable to be acquired at the same slice position, so the images were reconstructed with fine slice increments and the time increment for each image could be calculated using a transformation equation. In the present study, we adapted this approach for non-helical scanning, in which the continuously scanned dynamic data allows the acquisition of images with the same slice position at arbitrary time intervals. Thus, when plotting the TSP, the image reconstruction interval on the time axis is synonymous with the temporal sampling interval.

In the present study, a metal ball (11-mm in diameter) was shot from a launcher at high speed along the longitudinal axis at the center of the gantry (Fig. 1), and dynamic NVS was acquired as the ball passed through the axial plane. The average velocity of the metal ball was 11.6 ± 0.3 m/s, which was described in our previous study. Image reconstruction from the continuous NVS data was performed at 10- or 20-ms time intervals. Some reconstructed images included a streak artifact caused by the metal ball passing through. The CT value

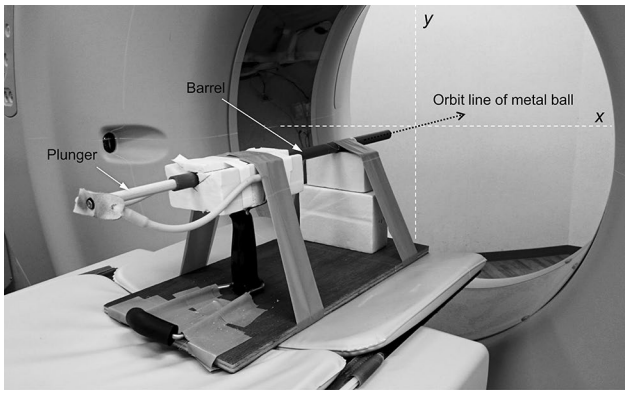

Fig. 1 Photograph of the metal ball launcher for TSP measurement. A metal ball passed through the barrel and was launched at high speed along the z-direction (black dash arrow)

of this artifact corresponds to the impulse response in the temporal domain, allowing the TSP to be generated by measuring the CT values of the streaks. A 40-pixel circular region of interest (ROI) was set at the center of each streak image and the CT values corresponding to the temporal responses were measured and plotted as the TSP (Fig. 2). The full width at half maximum (FWHM) and full width at tenth maximum (FWTM) of the TSP curves were measured. FWHM was used as an index of the eTR for the three reconstruction modes.

Image noise

Image noise was evaluated by measuring the standard deviation (SD) of CT value (in Hounsfield units, HU). The CTP712 Uniformity Module of a Catphan 700 phantom (Phantom Laboratory, New York, USA) was positioned at the isocenter with its cross-section parallel to the in-plane. CT values within a 120-mm diameter circular ROI placed at the center of the phantom images were measured 10 times for each condition and used to calculate the SD values.

Artifact index

As an assessment of artifacts similar to respiratory motion in chest CT, a rod phantom 50 mm in diameter was scanned as it moved along the *y*-axis at 10 mm/s, and the images were used to calculate the artifact index (AI), an index of motion artifact including both streaks and blurring. The CT value of the rod phantom was 90 HU, and that of the background was − 1000 HU. Figure 3 shows the acquired images of the rod with the circular ROIs (60 mm in diameter) placed for the AI calculation. The AI was calculated using the following equation [14]:

$$AI = \sqrt{\sigma_a^2 - \sigma_b^2}, \quad (1)$$

where σ_a is the SD of the mean CT values for ROIs 1 to 6, defined as the pixel amplitude with artifact, and σ_b is the SD of the mean CT values for ROIs 7 to 12, defined as the pixel

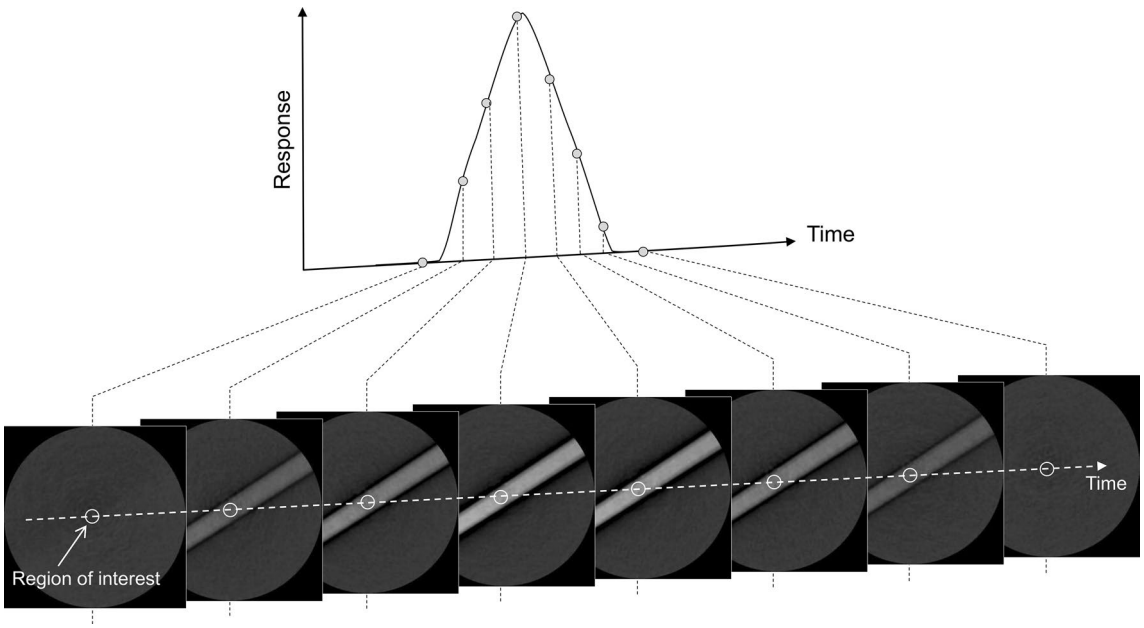

Fig. 2 Measurement of the temporal sensitivity profile using the impulse method. Circular regions of interest were placed on the streak images resulting from a metal ball passed through the scanning area. The temporal sensitivity profile was obtained by measuring the CT values of the streaks at the same slice position along the temporal direction

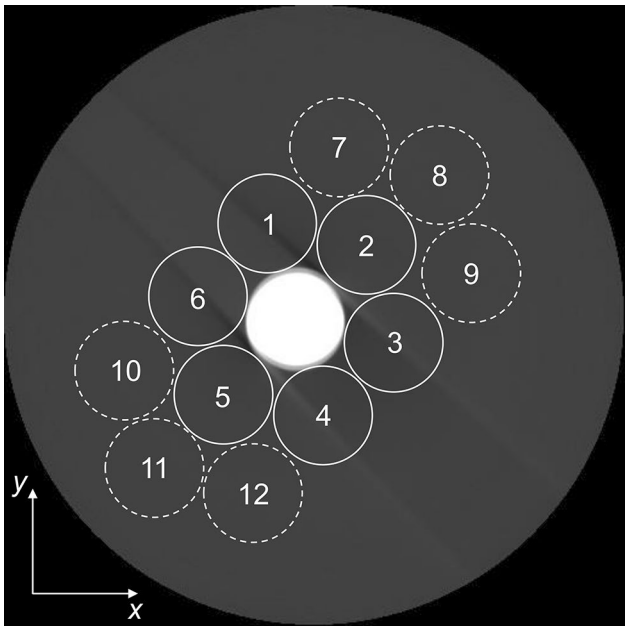

Fig. 3 Measurement of the artifact index using a moving rod phantom. Regions of interest (ROIs) 50 mm in diameter were place on the image of the moving rod. The artifact index was calculated from the standard deviation (SD) of the mean CT values obtained from ROIs 1 to 6, defined as amplitudes of CT value with artifact (σ_a), and the SD value of averaged CT value of ROIs 7 to 12, defined as amplitudes of CT value without artifact (σ_b)

amplitude without artifact (Fig. 3). To eliminate the influence of image noise, corrected AI (*cAI*) was calculated by multiplying AI by the coefficient of the background image noise:

$$cAI = n \cdot AI, \tag{2}$$

where n is expressed as the noise ratio of the target image to the full-reconstruction image,

$$n = SD_{full}/SD_{target}, \tag{3}$$

where SD_{full} is the SD of σ_b for the full reconstruction mode and SD_{target} is the SD of σ_b for the respective reconstruction mode.

Statistical analysis

Linear regression analyses were performed to determine the associations between the image noise and the FWHM and FWTM of the TSP curve. Because photon noise in a linear system is proportional to the reciprocal of the square root of the dose, the horizontal axis was denoted by the square root of FWHM and FWTM, respectively. For each regression, the adjusted coefficient of determination (R^2) was used as a goodness-of-fit measure. For the statistical analyses in this study, the null hypothesis was rejected at $P < 0.05$. The statistical analyses were performed with EZR software version 1.36 [15].

Results

Figure 4 shows the TSP graphs obtained with gantry rotation times of 275 and 400 ms and the three reconstruction modes. These were rectangular in shape for the full reconstruction mode, triangular for APMC, and convex for the half reconstruction mode. Table 1 shows the eTR and FWTM values for the three reconstruction modes and two rotation times. Full mode was the lowest in eTR and FWTM, followed by APMC and half mode.

Table 2 shows the image noise values for the three reconstruction modes and two rotation times. The image noise with APMC and half reconstruction were approximately 16% and 35% higher than that with full reconstruction.

Figure 5 shows the images of the moving rod phantom obtained with three reconstruction modes, and Table 3 shows the calculated AI and cAI values. The cAI values obtained with 275 ms rotation were lower than those with 400 ms rotation. At 275 ms rotation, cAI was lower for the APMC reconstruction than for the full and half reconstructions.

Figure 6 shows the predictability of the image noise according to the square root of FWHM and FWTM values obtained from the TSP curve. Linear regression analyses of the relationship between image noise and FWHM and FWTM showed that FWTM had the higher coefficient of determination, with R^2 values of 0.787 ($P = 0.018$) for FWHM and 0.934 ($P = 0.002$) for FWTM.

Discussion

To our knowledge, this is the first study that documents relationship between eTR and image quality for the three reconstruction modes of NVS in an area detector CT. The results revealed the eTR values and the shapes of the TSPs for each reconstruction mode, with eTR differing between the modes and between the two rotation times. In our previous study with helical acquisition [8], eTR depended on the rotation time, pitch factor, and interpolation algorithm, and image blur associated with the moving phantom improved with the scan parameters for a high eTR. In the present study, the motion artifact was improved by setting a short rotation time. Although the eTR was slightly lower with APMC than with the half reconstruction mode, the cAI value was smaller. Our results showed that the triangular shape of the TSP with APMC was effective for reducing artifacts due to the moving object.

Because the TSP of conventional step-and-shoot scanning with full reconstruction is rectangular shape, the rotation

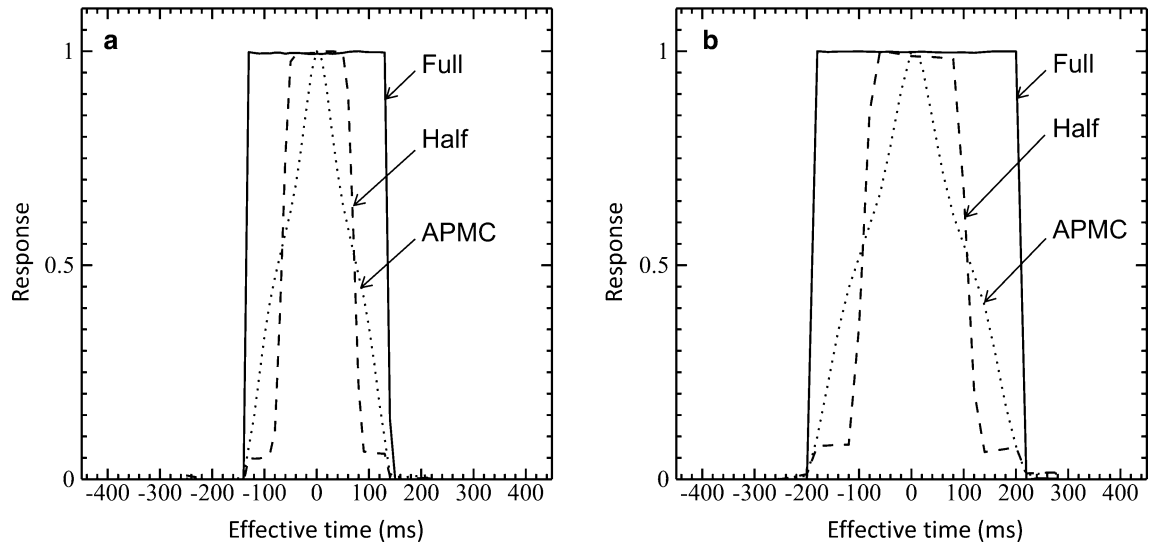

Fig. 4 The temporal sensitivity profile (TSP) graphs obtained with gantry rotation times of 275 (**a**) and 400 ms (**b**). The shape of the TSP was rectangular for the full reconstruction mode, triangular for automatic patient motion collection (APMC), and convex for the half reconstruction mode

Table 1 Full width at half and tenth maximums for three reconstruction modes and two rotation times

Rotation time (ms)	Full	APMC	Half
Full width at half maximum (ms)			
275	271	150	139
400	400	219	158
Full width at tenth maximum (ms)			
275	282	256	170
400	416	375	254

Full width at half maximum was used as an index of the effective temporal resolution for the three reconstruction modes

Full full reconstruction mode, *APMC* automatic patient motion collection, *Half* half reconstruction mode

Table 2 Image noise for the three reconstruction modes and two rotation times

Rotation time (ms)	Image noise (HU)		
	Full	APMC	Half
275	13.7 ± 0.10	15.8 ± 0.17	18.6 ± 0.21
400	11.4 ± 0.05	13.2 ± 0.05	15.5 ± 0.07

Full full reconstruction mode, *APMC* automatic patient motion collection, *Half* half reconstruction mode

time and eTR can be considered to be the same. In contrast, various image reconstruction algorithms are applied to NVS acquisition with ADCT to improve image quality and temporal resolution. Taguchi et al. [16] proposed four different Feldkamp-based algorithms for dynamic volumetric imaging, and evaluated the image quality and temporal resolution for these. With a moving object, the image quality and temporal resolution depended on the weighting function of the reconstruction algorithm. In our study, the reconstruction algorithm with the highest eTR (half reconstruction) showed higher image noise compared to the full reconstruction mode with the same raw data because it used only limited projection data in the temporal domain. Furthermore, the streak artifact resulting from the motion of the object was greatly influenced by the shape of the TSP; the triangular-shaped TSP (with APMC) was effective in reducing streak artifacts. Thus, APMC would be clinically effective when scanning moving organs and in dynamic four-dimensional examinations. Kunitomi et al. [17] reported that image reconstruction by APMC was effective for reducing misregistration in cerebral four-dimensional CT-angiography. Their results were consistent with those of the present study.

The linear regression analysis of image noise showed a high coefficient of determination for the FWTM of the TSP. This suggests that TSP is effective not only as an index of actual temporal resolution but also as an index of image noise, corresponding to the weighting function of the projection data in NVS. However, because the image noise reflects the utilization efficiency of the projection data in the temporal domain corresponding

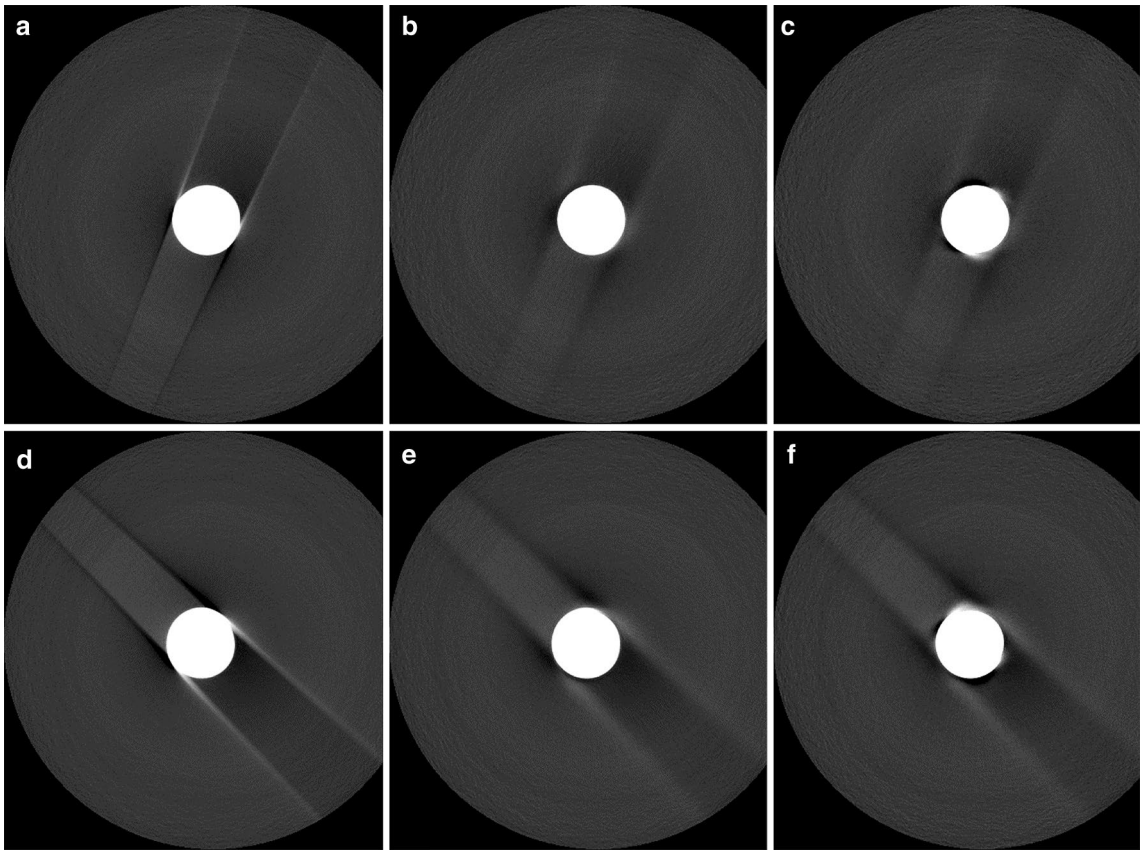

Fig. 5 Rod images acquired by full (**a, d**), automatic patient motion collection (APMC) (**b, e**), and half (**c, f**) reconstruction with gantry rotation times of 275 ms (upper row) and 400 ms (lower row). The window width and center settings were adjusted to 800 and −750 Hounsfield units. The streak artifact and blur were better with the 275 ms rotation than with the 400 ms rotation, with the APMC image for the 275 ms rotation showing significantly improved streak and blur

Table 3 Artifact index and corrected artifact index values measured using a moving rod phantom

Rotation time (ms)	Full	APMC	Half
Artifact index			
275	7.2	6.0	8.3
400	15.3	12.0	15.2
Corrected artifact index			
275	7.2	5.2	6.4
400	15.3	10.5	11.8

Full full reconstruction mode, *APMC* automatic patient motion collection, *Half* half reconstruction mode

to the weighting function of the interpolation algorithm [16], the FWTM alone obtained from the TSP may not sufficiently reflect the overall temporal element in the CT images. In particular, it is unclear whether similar results can be obtained with helical acquisition performed using advanced CT scanners, which have complicated interpolation algorithms. Thus, although the detailed relationship between TSP shape and image noise should be considered, characterization of the TSP was partly possible for using the FWTM as an index for image noise prediction. Our results showed that foot spreading of the TSP profile was effective in reducing image noise while improving the temporal resolution. To maintain the image quality while reducing motion artifacts, CT operator should determine the optimal reconstruction mode.

Kawaguchi et al. [18] assessed image quality with the three reconstruction modes for CCTA using an Aquilion ONE scanner. They suggested that, compared to the half reconstruction mode commonly used in CCTA, the use of APMC or full reconstruction could reduce the radiation dose while maintaining a clinical diagnostic performance. These two modes resulted in lower image noise than with half reconstruction, even with radiation doses that were 30% (for APMC) and 50% (for full reconstruction) lower. However, their study used a hybrid iterative algorithm for image reconstructions. It is therefore difficult to directly compare relationships between radiation dose and image noise [19, 20], but their results were similar to the trend

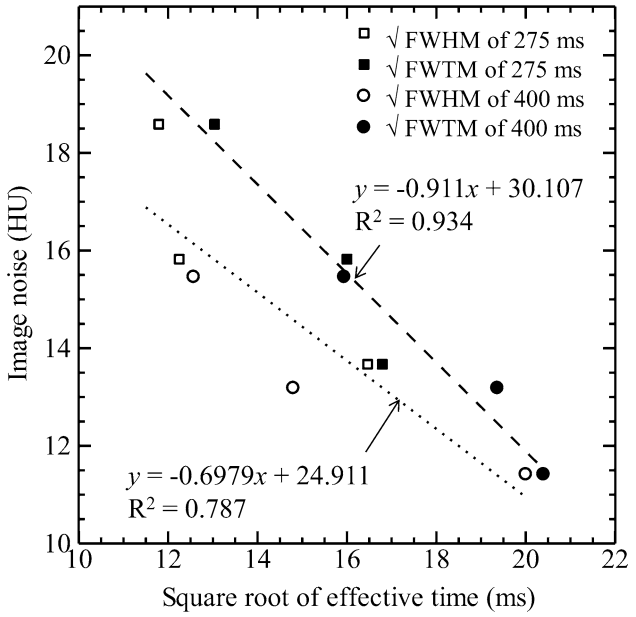

Fig. 6 The predictability of image noise using square root of full width at half maximum (FWHM) and full width at tenth maximum (FWTM) of the temporal sensitivity profile curve. The dotted and dashed lines indicate the regression lines for the FWHM and FWTM plots, respectively. Linear regression analysis yielded R^2 values of 0.787 and 0.934 for FWHM and FWTM, respectively

for an association between image noise and the FWTM from the TSP curve showed in the present study.

Our study had several potential limitations. It was a phantom study performed with an ADCT scanner from a single vendor. Various interpolation algorithms are employed in other advanced ADCT scanners, and so these may exhibit different TSP shapes and image noise tendencies. In addition, our study did not include assessments of clinical images. The impact on motion artifacts and image noise in clinical images will be addressed in a future study.

In conclusion, this study revealed the TSP shapes and eTR values for NVS with three reconstruction modes. Motion artifact was improved by setting a short rotation time and using a reconstruction mode that produces a high eTR. Although APMC was associated with a lower eTR compared to the half reconstruction mode, it had a lower cAI. The half reconstruction algorithm with a high eTR showed higher image noise compared to the full reconstruction mode with same raw data because it used only limited projection data in temporal domain.

Funding This research did not receive any specific grant from funding agencies in the public, commercial, or not-for-profit sectors.

Compliance with ethical standards

Conflict of interest The authors declare that they have no conflict of interest.

Ethical approval Institutional review board approval was not required for this phantom study.

References

1. Ko SF, Hsieh MJ, Chen MC, Ng SH, Fang FM, Huang CC et al (2005) Effects of heart rate on motion artifacts of the aorta on non-ECG-assisted 0.5-sec thoracic MDCT. Am J Roentgenol 184:1225–1230
2. Kim SH, Choi YH, Cho HH, Lee SM, Shin SM, Cheon JE et al (2016) Comparison of image quality and radiation dose between high-pitch mode and low-pitch mode spiral chest ct in small uncooperative children: the effect of respiratory rate. Eur Radiol 26:1149–1158
3. Sandfort V, Ahlman MA, Jones EC, Selwaness M, Chen MY, Folio LR et al (2016) High pitch third generation dual-source CT: coronary and cardiac visualization on routine chest CT. J Cardiovasc Comput Tomogr 10:282–288
4. Liang T, McLaughlin P, Arepalli CD, Louis LJ, Bilawich AM, Mayo J et al (2016) Dual-source CT in blunt trauma patients: elimination of diaphragmatic motion using high-pitch spiral technique. Emerg Radiol 23:127–132
5. Ohashi K, Ichikawa K, Hara M, Kawai T, Kunitomo H, Higashide R et al (2013) Examination of the optimal temporal resolution required for computed tomography coronary angiography. Radiol Phys Technol 6:453–460
6. Hutt A, Tacelli N, Faivre JB, Flohr T, Duhamel A, Remy J et al (2016) Is bronchial wall imaging affected by temporal resolution? comparative evaluation at 140 and 75 ms in 90 patients. Eur Radiol 26:469–477
7. Taguchi K, Anno H (2000) High temporal resolution for multislice helical computed tomography. Med Phys 27:861–872
8. Ichikawa K, Hara T, Urikura A, Takata T, Ohashi K (2015) Assessment of temporal resolution of multi-detector row computed tomography in helical acquisition mode using the impulse method. Phys Med 31:374–381
9. Hara T, Urikura A, Ichikawa K, Hoshino T, Nishimaru E, Niwa S (2016) Temporal resolution measurement of 128-slice dual source and 320-row area detector computed tomography scanners in helical acquisition mode using the impulse method. Phys Med 32:625–630
10. Yamashiro T, Miyara T, Takahashi M, Kikuyama A, Kamiya H, Koyama H et al (2012) Lung image quality with 320-row wide-volume CT scans: the effect of prospective ECG-gating and comparisons with 64-row helical CT scans. Acad Radiol 19:380–388
11. Honda O, Takenaka D, Matsuki M, Koyama M, Tomiyama N, Murata K et al (2012) Image quality of 320-detector row wide-volume computed tomography with diffuse lung diseases: comparison with 64-detector row helical CT. J Comput Assist 36:505–511
12. Kroft LJ, Roelofs JJ, Geleijns J (2010) Scan time and patient dose for thoracic imaging in neonates and small children using axial volumetric 320-detector row CT compared to helical 64-, 32-, and 16-detector row CT acquisitions. Pediatr Radiol 40:294–300
13. Mahesh M (2011) Advances in CT technology and application to pediatric imaging. Pediatr Radiol 41(Suppl 2):493–497
14. Wang Y, Qian B, Li B, Qin G, Zhou Z, Qiu Y et al (2013) Metal artifacts reduction using monochromatic images from spectral

CT: evaluation of pedicle screws in patients with scoliosis. Eur J Radiol 82:e360–e366
15. Kanda Y (2013) Investigation of the freely available easy-to-use software 'EZR' for medical statistics. Bone Marrow Transplant 48:452–458
16. Taguchi K (2003) Temporal resolution and the evaluation of candidate algorithms for four-dimensional CT. Med Phys 30:640–650
17. Kunitomi Y, Watanabe Y, Arisawa A, Tsukabe A, Tanaka H, Takahashi H et al (2016) Reduction of misregistration on cerebral four-dimensional computed tomography angiography images using advanced patient motion correction reconstruction. Jpn J Radiol 34:605–610
18. Kawaguchi Y, Fujimoto S, Takamura K, Kato E, Suda S, Matsumori R et al (2018) Submillisievert imaging protocol using full reconstruction and advanced patient motion correction in 320-row area detector coronary CT angiography. Int J Cardiovasc Imaging 34:465–474
19. Love A, Olsson ML, Siemund R, Stålhammar F, Björkman-Burtscher IM, Söderberg M (2013) Six iterative reconstruction algorithms in brain CT: a phantom study on image quality at different radiation dose levels. Br J Radiol 86:20130388
20. Urikura A, Hara T, Ichikawa K, Nishimaru E, Hoshino T, Yoshida T et al (2016) Objective assessment of low-contrast computed tomography images with iterative reconstruction. Phys Med 32:992–998